Materials and Structures (2021)54:244
https://doi.org/10.1617/s11527-021-01838-z

ORIGINAL ARTICLE

The influence of the chemical composition of hydrogels on their behavior in cementitious materials

Khashayar Farzanian · Babak Vafaei · Ali Ghahremaninezhad

Received: 27 March 2021 / Accepted: 4 December 2021

Abstract This study examines how the chemical composition of hydrogels influences the behavior of hydrogels in cementitious materials. A stark contrast in the behavior of some hydrogels in extracted cement pore solution, where cement particles are excluded, and in cement mixture was observed. The observed contrast was attributed to the chemical processes between the hydrogel and cement particles, which are excluded in the extracted pore solution. This finding raises concerns regarding the accuracy of hydrogel absorption measurements using only the extracted pore solution to determine the absorption of hydrogels in cement paste. The effect of hydrogels with different chemical compositions on the hydration, electrical resistivity, autogenous shrinkage, and strength of cement paste was evaluated and discussed.

Keywords Hydrogel · Chemical interactions · Absorption · Cementitious materials

K. Farzanian · B. Vafaei · A. Ghahremaninezhad (✉)
Department of Civil, Architectural and Environmental Engineering, University of Miami, Coral Gables, FL 33146, USA
e-mail: a.ghahremani@miami.edu

Present Address:
K. Farzanian
Department of Internal Medicine, Yale University, New Haven, CT 06511, USA

Published online: 15 December 2021

1 Introduction

Cracking due to autogenous shrinkage remains a challenge in high performance concrete (HPC), which is formulated with a low water/cement (w/c) [1–8]. In HPC, with continued hydration and consumption of water, internal relative humidity gradually decreases (self-desiccation) and capillary tension is developed in the menisci in the pores. The capillary tension in the pore solution pulls inward on the solid skeleton and this manifests as the overall shrinkage of the material [9, 10]. In presence of constraint in the material, e.g. provided by aggregates, autogenous shrinkage causes tensile stress, which could lead to crack formation [10]. Once cracks are formed, the transport of deleterious agents into the interior of the material accelerates, which can lead to a number of deterioration processes including reinforcing steel corrosion, and chemical and physical attacks [11].

Traditional curing methods, such as providing water from the surface, are not effective in reducing autogenous shrinkage in cementitious materials since autogenous shrinkage occurs over the volume of the material unlike the drying shrinkage, which takes place due to loss of water at the surface [5]. Internal curing has proven to be an effective means to reduce autogenous shrinkage in cementitious materials [2, 3, 5, 9, 12–22]. In internal curing, water is provided from internal sources into the cementitious matrix to maintain internal relative humidity during hydration

[9]. Examples of the materials used for internal curing include pumice, superabsorbent polymers (SAP), and saturated lightweight aggregates [23]. In particular in recent years, SAP has emerged as an effective material to reduce autogenous shrinkage in cementitious mixtures [3, 5, 9, 16, 17, 24].

In addition to reducing autogenous shrinkage, SAP has been found to enhance hydration [13, 25, 26], increase resistance to chloride penetration [12, 13], improve freeze–thaw resistance [27], and induce self-healing [28–30] in cementitious materials. While in several prior studies compressive strength has been shown to be reduced in the presence of SAP due primarily to the macrovoid formation [5, 15, 31–33], there have also been investigations where the use of SAP increased compressive strength [34]. Mixture formulation and the physicochemical characteristics of SAP are factors directly influencing how SAP affects the behavior of cementitious materials [5, 8, 12, 14, 32].

SAP utilized in the cementitious materials is a hydrogel, typically comprised of a crosslinked polymer of acrylate salt or copolymer of acrylate salt—acrylamide [3, 14, 22, 35]. These hydrogels are polyelectrolyte and their response depends on stimuli including ionic composition and pH [5, 31, 32, 35–40].

The knowledge of hydrogel behavior including its absorption and desorption in cementitious materials is necessary to understand how they affect the properties and microstructure of cementitious materials. For example, compressive strength is strongly affected by the size of macrovoids left in microstructure and this is governed by the absorption behavior of hydrogels [32]. In addition, the desorption behavior of hydrogels has an effect on the autogenous shrinkage of cementitious materials [5, 17]. Since many properties of cementitious materials are strongly dependent on w/c, an accurate determination of hydrogel absorption is of paramount importance.

The absorption behavior of hydrogels is typically determined (1) in a direct way in a solution using the teabag test [16, 17, 32, 41–43], or (2) in an indirect way in cement mixture using the flowability measurement [1, 5, 40, 44, 45]. Direct absorption measurement in a solution is based on mass or volume change of the hydrogels in the solution. In the indirect absorption determination using the flowability measurement, additional water is added to the cement mixture to obtain the same flow value for the mixture with and without hydrogel; in this method, the additional water is assumed to be absorbed by the hydrogel and not contribute to the flow value of the mixture.

Various test methods to measure the absorption of hydrogel in solutions have been discussed in a review paper [46]. A recent round robin study examined the absorption of hydrogels in cement pore solutions using the teabag method and filtration method, and pointed out the strengths and weaknesses of each method [47]. Other investigations employed optical imaging [35, 48] or laser light diffraction [49] to measure the hydrogel absorption in a solution. Few studies examined the absorption of hydrogels in a cementitious mixture, rather than in a solution, in a direct way using optical microscopy [50–52], scanning electron microscopy [53], and neutron radiography [43]. Due to their simplicity, the teabag test and flow test have been the most widely used methods to estimate the absorption of hydrogels relevant to cementitious materials.

However, a comparison between the above-mentioned absorption measurement methods is lacking in the literatures, which impedes an assessment of each method's reliability to yield accurate absorption results. In this paper the absorption of hydrogels with different chemical compositions in a pore solution and in a cement mixture was studied. Surprisingly, some hydrogels demonstrated a significant difference in their absorption response in a pore solution and in a cement mixture. This paper aims to address a knowledge gap in understanding the factors affecting the absorption of hydrogels in cement mixtures beyond the well-established chemical interaction between the pore solution and hydrogels.

A detailed study was carried out in this paper to understand the underlying mechanisms responsible for such a peculiar behavior of the hydrogels. Since the hydrating solid particles are filtered out and not present in the pore solution, their potential interactions with hydrogels could be responsible for the stark difference in hydrogel absorption in the pore solution and in the cement mixture. Thus, the physical and chemical processes occurring between the hydrogels and solid particles in a mixture were systematically investigated in this study. In the remaining part of the paper, the desorption behavior of the hydrogels was also examined. The effect of the hydrogels on the autogenous shrinkage, hydration, electrical resistivity, and compressive strength of cement pastes was also evaluated and discussed.

2 Experiments

2.1 Materials

2.1.1 Hydrogels

In this study, three hydrogels with different chemical compositions were prepared in-house and utilized in the experiments. All chemicals used in synthesizing hydrogels were purchased from Sigma-Aldrich. The chemical compositions of the hydrogels synthetized in this study and their designations are shown in Table 1. The main monomers used in the hydrogels were acrylic acid (AA) and acrylamide (AM) and the synthesis was carried out using the free radical polymerization, as detailed in our previous papers [37, 54, 55]. First, AA was dissolved in 50 mL volume of distilled water and then sodium hydroxide (NaOH) was used to achieve a partial neutralization of AA. AM and 0.025 g of *N,N'*-methylenebisacrylamide (MBA), which serves as a crosslinking agent, were added to the solution and stirred for 30 min to ensure complete dissolution. Then, argon gas was used to sparge the solution for 3–5 min to remove dissolved gases. Ammonium persulfate (APS) as the polymerization initiator in the amount of 0.064 g was added to the solution. AA and NaOH were not used in synthesizing Hyd-c; for this hydrogel after dissolving AM and MBA in the solution, 0.3 g of sodium alginate (Alg) was added and stirred for 24 h due to the slow dissolution of sodium alginate in the solution. The dissolved oxygen was removed by argon in the next day and APS was added to the solution.

The solutions were poured into glass molds of different sizes and transferred into an oven at 60 °C for 3 h to allow gelation to occur. Then, the hydrogels were demolded, broken into smaller pieces, and submerged in distilled water for 24 h. In the case of Hyd-c instead of distilled water, pieces of hydrogel were submerged in an ionic solution prepared following the composition of an artificial pore solution used by Tunstall et al. 2017 [56]. The ionic solution contained 0.1062 M KOH, 0.0489 M Na_2SO_4, 0.037 M K_2SO_4, and 0.0212 M $Ca(OH)_2$ [56]. It should be noted that Hyd-b and Hyd-c have a similar chemical composition as shown in Table 1. The reason for submerging Hyd-c in the ionic solution was to allow penetration of ionic species, commonly present in cement pore solution, into the hydrogels. The presence of these ions in the hydrogel affects the molecular structure of this hydrogel through ionic crosslinking and also affects the chemical composition of the counterions in the hydrogels. Thus, Hyd-c is expected to show a different behavior, compared to Hyd-b.

After 24 h of submersion in the solution, the hydrogels were washed and then dried in an oven at 60 °C for one week to be fully dried. Dried pieces of hydrogels were then ground into a powder using a coffee grinder and sieved using a shaker (RX-29, WS TYLER). The hydrogel particles passing through the sieve # 50 (300 μm) and remaining on the sieve # 200 (75 μm) were used in the cement paste. The hydrogel powders were sealed in double-layer polyethylene bags and stored in a desiccator to prevent moisture uptake.

Specific molds were used to prepare hydrogel disks and microstrips for use in the Fourier transform infrared spectroscopy (FTIR) and desorption tests, as detailed later in the paper. These molds consisted of two rectangular glass plates sandwiching a rubber gasket with different thicknesses of 0.5 and 3.5 mm. Using these molds was necessary to prepare hydrogel samples with smooth surfaces needed for the FTIR and desorption tests. After the gelation process of 3 h in the oven, the hydrogel layers were removed from the glass molds and their surfaces were cleaned using alcohol to remove residual/unreacted monomers from the surface. In order for the surface of hydrogel layers to be without any wrinkles or creases, Hyd-a and Hyd-

Table 1 Compositions of the hydrogels used in the experiment

Hydrogel designation	Distilled water (g)	AA (g)	AM (g)	Alg (g)	NaOH (g)	MBA (g)	APS (g)
Hyd-a	50	5	5	–	0.675	0.025	0.064
Hyd-b	50	1	9	–	0.135	0.025	0.064
Hyd-c	50	–	10	0.3	–	0.025	0.064

b layers were immersed in distilled water and Hyd-c layer in ionic solution, respectively, for approximately 2–3 h until all wrinkles and creases disappeared and a smooth surface was obtained. For the FTIR test, the hydrogel disks were punched from the hydrogel layers using a circular punch. For the desorption test, narrow microstrips were cut using a razor blade. Both hydrogel disks and microstrips were dried in an oven at 60 °C. The final dry hydrogel disks had a thickness of 1.7 mm and a diameter of 9 mm and the final dry hydrogel microstrips had a thickness of 0.32 mm, width of 0.62 mm, and length of 50 mm.

2.1.2 Cement mix design

A type I/II Portland cement was used in producing the pastes. The chemical characteristics of the cement are shown in Table 2. The mix designs of the cement pastes used in the experiments are listed in Table 3. The mix design used in the teabag test and the FTIR analysis is descried in the respective sections. Control paste without hydrogels, and pastes containing 0.3%, per cement mass, of Hyd-a and Hyd-b, and 0.6%, per cement mass, of Hyd-c were prepared. The reason for a different amount of Hyd-c compared to that of Hyd-a and Hyd-b used in the cement pastes was to obtain the same total w/c in the cement pastes with Hyd-b and Hyd-c. This allowed for comparing the effect of these two hydrogels while maintaining the total w/c of the pastes. Dry hydrogel powder was first dry mixed with cement for 5 min using a mixer. In order to increase workability, a superplasticizer (WRDA 60, W. R. Grace & Co.-Conn.) at a concentration of 0.5%, per cement mass, was added to the water. Then, cement and SAP were mixed with water containing the superplasticizer in a bucket for 30 s at a speed of 440 RPM. After pausing for 15 s to scrape the inside wall of the bucket, the mixing continued at a speed of 1600 RPM for 60 s. The paste was then immediately poured into cubic molds (50 × 50 × 50 mm) in two layers. Each layer was tamped per the ASTM C 109. In order to protect the pastes from evaporation, the molds were wrapped with a pre-stretch plastic foils and stored in double-layer polyethylene bags. The cubes were demolded after 24 h and immediately stored in double-layer bags.

Table 2 Oxide composition of cement

Composition	(%)
SiO_2	20.6
Al_2O_3	4.8
Fe_2O_3	3.5
CaO	64
MgO	0.9
Na_2O	0.1
K_2O	0.3
SO_3	3.4
LOI	2.4

2.2 Experimental methods

2.2.1 Hydrogel absorption in extracted pore solution using the teabag test

Hydrogel absorption in the extracted pore solution was measured using the teabag test. A cement mixture with a w/c of 0.6 was prepared. Since a superplasticizer was used in the preparation of all cement mixtures in this study, the superplasticizer at a concentration of 0.5%, per cement mass, was added to water. Approximately 60 min after water and cement came into contact, the mixture was loaded in a filtration setup to extract the pore solution under a negative pressure. The extracted pore solution was immediately transferred into polypropylene tubes to prevent being exposed to air. Approximately 0.1 g of each hydrogel powder was placed in three teabags and immersed into the solution medium. The teabags were removed from the solution at specific time intervals, their surfaces dried gently, and their mass measured using an analytical balance with the 0.001 g resolution. Hydrogel absorption was determined as follows.

$$Q = \frac{M_w - M_{wt} - M_s}{M_s} \quad (1)$$

where M_w, M_{wt}, and M_s are the mass of the wet teabag containing hydrogels, wet teabag without hydrogels, and dry hydrogel, respectively. The teabags were immediately returned to the solution to minimize exposure to air and the solution was sealed with Parafilm. To account for the amount of the solution absorbed by the teabags, the mass of the wet teabag without hydrogel (M_{wt}) was determined by submerging several dry teabags without hydrogel in the solution and their average mass was determined. The absorption measurements in the extracted pore solution was conducted until 80 min.

Table 3 Mix designs of the cement pastes used in the experiments

Paste designation	W/C	Superplasticizer (% per cement mass)	Hydrogel (% per cement mass)	Flow (cm)	Absorption (g/g dry)		
					Hyd-a	Hyd-b	Hyd-c
C	0.35	0.5	–	24			
C Hyd-a	0.38	0.5	0.3	24	10		
C Hyd-b	0.47	0.5	0.3	24		40	
C Hyd-c	0.38	0.5	0.6	24			5

2.2.2 *Flow test*

The flow test of the cement pastes was performed per the ASTM C1437. The effective w/c of 0.35 was considered in all cement pastes. In this test, a cone (top diameter: 70 mm, bottom diameter: 100 mm, and height: 50 mm) was filled with paste and allowed to sit on a table for 10 min. Then, the test followed by removing the cone and repeated dropping of the table 25 times with the same rate in a time span of 15 s. The diametrical dimensions of the paste were determined and used to estimate the flow value. The flow test was repeated two times on the control paste without hydrogels (C) and the average flow value was determined to be 24 cm. For the pastes with hydrogels, additional water in the increments of $\delta(w/c) = 0.02–0.03$ was added to the paste to obtain the same flow value of 24 cm as for the control paste. The flow test was also repeated twice for the cement pastes with hydrogels and the average was reported. The additional water was assumed to be absorbed by the hydrogels and used to obtain an indirect estimate of hydrogel absorption.

To investigate the effect of the type of solid particle, the behavior of hydrogels in different mixtures containing fly ash (FA) and glass powder (GP) were studied. FA and GP were used as these particles are expected to be inert or less reacting in the first 10 min of being in contact with solution and this time corresponds to the time at which the flow test was carried out. The ionic solution with composition similar to an artificial pore solution as described in [56] was used in the preparation of FA and GP mixtures. The reason for using the ionic solution in these mixtures was to maintain a similar solution chemistry in the mixtures and to allow us to focus on the effect of solid particles on the absorption of hydrogels. The mixtures used in the flow test were prepared with the same dosages of superplasticizer and hydrogel as in the cement mixtures. The same flow value target of 24 cm as in the cement mixtures was used in determining the solution/solid of the FA and GP mixtures with and without hydrogels.

2.2.3 *Modified teabag test*

Additionally, we performed a modified teabag test by submerging into the ionic solution a larger teabag containing a dry mixture of solid particles and hydrogel. Approximately 0.5 g of hydrogel and 10 g of cement, FA, and GP, were dry mixed for 5 min and then placed in separate teabags. In the case of cement, water instead of the ionic solution was used. The test was also conducted using solid particles without hydrogel to measure the absorption of the solid particles and this was subtracted from the absorption of solid particle and hydrogel to determine the absorption of hydrogel. The tests were conducted with 3 replicates. The reason for the modified teabag test was to include the effect of interactions between the solid particles and hydrogel.

2.2.4 *X-Ray micro-computed tomography (micro-CT)*

X-ray micro-CT was used to study the size of the macrovoids formed as the result of hydrogel absorption. The size of the macrovoids represents the largest hydrogel absorption before the cement paste was set. To this end, cement paste prisms with the dimension of $25 \times 25 \times 285$ mm following the same mix design as with the cement paste cubes were prepared (see Table 3). At the age of 28 days, samples with the dimensions of $25 \times 25 \times 25$ mm were cut from the prisms using a saw, soaked in acetone, vacuum oven dried at a temperature of 60 °C for 48 h and stored in a desiccator until scanning. The samples were scanned

using a SkyScan 1273 (Bruker) with a voltage of 130 kV and current of 115 μA. The resolution was 15° m/pixel. An x-ray exposure time of 342 ms and a rotational step of 0.15° were selected. The macrovoid size analysis was performed using CTAnalyzer 1.20.8 (Bruker). A 10 mm cylindrical volume from the center of the samples was scanned and analyzed. Since the dry hydrogels used in the mixtures were sieved to have the same initial size range of 75–300 μm, only macrovoids larger than 75 μm were considered in the micro-CT analysis.

2.2.5 FTIR

FTIR was used to study how the interactions with extracted pore solution and cement mixtures affect the chemical characteristics of the hydrogels. Hydrogel disks were submerged in tubes containing extracted pore solution and in tubes that contained a cement mixture with a w/c of 2. The superplasticizer at 0.5% cement mass was added to the cement mixture. The tubes containing cement mixture were frequently shaken and rotated to ensure that the cement was not hardened in the tubes. Hydrogel disks were immersed in the tubes for 8 h and taken out only for performing the test. The FTIR scan was carried out on both surfaces of the hydrogel disks. A PerkinElmer Paragon 1000 FTIR with the ATR accessory was used.

2.2.6 Absorption under constraint

In order to investigate how physical constraint can influence the absorption behavior of hydrogels, we devised an experiment as seen in Fig. 1. In this experiment, the absorption of hydrogels in the ionic solution under three different pressure levels, 0, 0.75, and 1.5 kPa, was measured. Weights were used to apply different pressure levels on the hydrogels. The details of the experiment are provided in [32]. The absorption was calculated based on volumetric change.

2.2.7 Desorption of hydrogel

The desorption behavior of the hydrogel microstrips embedded in hydrating cement pastes was studied in this section. Plastic tubes (diameter: 30 mm and length: 120 mm) were first cut open in their axial direction so that cement paste could be poured into the tubes. First, the bottom half of the tubes was filled with cement paste and then a single hydrogel microstrip was placed on the paste and allowed to uptake solution from the paste for 5–10 min. Wrinkles were noted to form in the hydrogel microstrips; in order to prevent the interference of the wrinkles with the measurement of the cross sectional dimensions, microstrips were carefully lifted up, de-wrinkled, and immediately put back over the paste surface. After filling the upper half of the tubes with the paste, the tubes were sealed. Sections perpendicular to the axis of the tubes were prepared at different time intervals and imaged by a micro-camera. In order to prevent water from coming into contact with the hydrogel microstrips and potentially altering them, the tubes were first sawed up to the mid-radius using a water-cooled saw and then broken into two parts manually to reveal the sections.

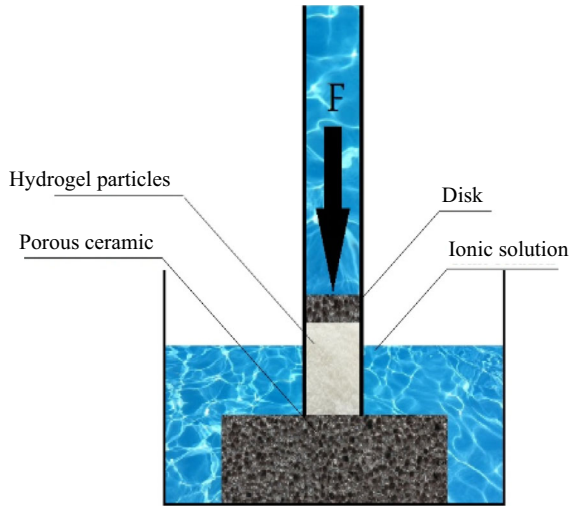

Fig. 1 Schematic of the setup used to study the effect of constraint on the absorption of hydrogels

In order to account for variability, more than five replicates were used in this experiment. The images were finally analyzed using the Imagej software and the hydrogel desorption was estimated as water loss as follows:

$$\text{Water loss} = 1 - \frac{a_t}{a_0} \tag{2}$$

where a_0 is the microstrip void area and a_t is the microstrip cross sectional area at time t. The void area represents the largest absorption of hydrogel microstrip.

2.2.8 Autogenous shrinkage

The autogenous shrinkage of the cement pastes was determined per the ASTM C1698-09. Long corrugated plastic tubes (length: 420 mm and outer diameter: 29 mm) were filled with each cement paste. Length change measurements of the tubes were taken every 12 h in the first week and continued once a day until the 30 days at room temperature (21 ± 2 °C). Measurement was started at the time coinciding with the final set of the pastes as measured by the Vicat test. Two replicates were used for each cement paste and the average was reported.

2.2.9 Electrical resistivity

In this study, the electrochemical impedance spectroscopy (EIS) technique was employed to determine the electrical resistivity of the cement pastes [57, 58]. EIS was performed using a Gamry Reference 600 potentiostat/galvanostat with a frequency domain of 10^6 to 10 Hz and signals of 250 mV. After drying the two surfaces of the cubes, they were placed between two conductive metallic plates. Two pieces of foam prewetted with a 1 M NaCl solution were placed between the cube surfaces and the conductive plates to ensure the conductivity at the interfaces. Electrical resistivity of five replicate cubes of each paste at three ages was measured and the average was reported. The electrical resistivity (ρ) is determined as follows:

$$\rho = (Re)(A)/(t) \tag{3}$$

where t, A, and Re are the cube thickness (m), surface area (m^2), and measured resistance (Ω), respectively.

2.2.10 Compressive strength

The compressive strength of the cement paste cubes was determined using a SATEC material testing instrument. Five replicate cubes of each paste were tested at three different ages of 3, 7, and 28 days and the average was reported.

2.2.11 Thermogravimetric analysis (TGA)

Samples for TGA were prepared by grinding the pieces from the center of the cubes broken in the compressive strength test, sieved using the Sieve No. 60, and vacuum dried at 50 °C for 24 h. Approximately 35 mg of the ground cement paste was scanned using the Netzsch TG at the heating rate of 20 °C /min and in the temperature range of 23–1000 °C. Mass reduction as a result of the conversion of calcium hydroxide into CaO and H_2O occurs in the temperatures between 400 and 500 °C. The amount of CH normalized with respect to the cement mass was determined as follows:

$$\mathrm{CH} = \frac{74.1}{18}\frac{MA}{MB} \tag{4}$$

where MB (mg) and MA (mg) are the initial mass of the sample and the change in mass due to the decomposition of calcium hydroxide, respectively. Two replicates were used for each cement paste at two ages of 3 and 28 days and the average was reported.

3 Results and discussion

3.1 Teabag test and flow test

The absorption behavior of the hydrogels in the extracted pore solution measured using the teabag test is illustrated in Fig. 2. The results showed the highest absorption for Hyd-b (27 g/g), while the lowest absorption was observed for Hyd-c (9 g/g), all measured at 80 min. Both Hyd-a and Hyd-c reached a plateau at about 5 min, but the Hyd-b absorption continued increasing after 5 min towards the end of the experiment but at a much lower rate. Pore solution in a cementitious mixture possesses various ions, including Na^+, K^+, Ca^{2+}, and OH^-, as a result of

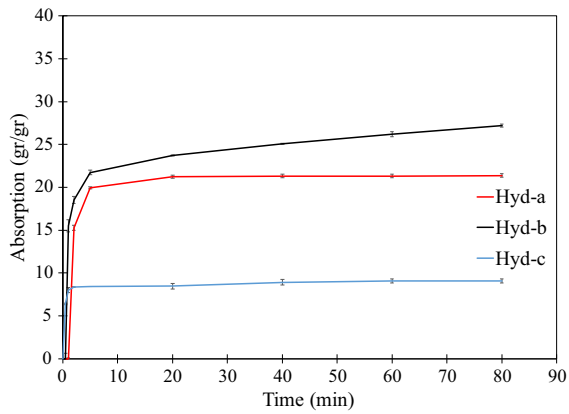

Fig. 2 Absorption of Hyd-a, Hyd-b, and Hyd-c in the extracted pre solution using the teabag test

cement dissolution and hydration. The cations present in the pore solution significantly affect the absorption of hydrogels as a result of charge screening and complex formation [5, 30, 36]. The absorption of hydrogels in synthetic pore solutions and extracted pore solutions was investigated by several researchers in the past [5, 31, 35]. Ionic concentrations and pH of the solutions have been shown to affect the hydrogel absorption [30, 39, 44]. The higher concentration of negatively charged AA in Hyd-a compared to Hyd-b could explain the slightly lower absorption of Hyd-a due to the complexation of the Ca^{2+} with anionic groups of the hydrogel network and screening effect of cations present in the pore solutions [5, 30, 36]. As expected, Hyd-c showed the lowest absorption compared to Hyd-a and Hyd-b; this behavior stemmed from the synthesis method used for this hydrogel where this hydrogel was previously submerged in an ionic solution for about 24 h after gelation. The long term prior exposure of Hyd-c to the ionic solution promoted the diffusion of cations present in the solution into Hyd-c and formation of ionic crosslinks between the negatively charged polymer network and Ca^{2+}, both of which resulting in a lower absorption capacity of Hyd-c when it was submerged into the extracted pore solution.

Absorption results obtained using the flow test is given in Table 3. The results showed an absorption of 10 (g/g), 40 (g/g), and 5 (g/g) for Hyd-a, Hyd-b, and Hyd-c, respectively. The absorption values are calculated based on the assumption that the added water to maintain the same flow values of the mixtures is absorbed by hydrogels.

Strikingly, a significant difference was observed in the absorption of Hyd-a and Hyd-b obtained from the teabag test and the flow test. While the difference in the absorption between Hyd-b and Hyd-a is about 12% in the teabag test measured at 20 min, it is about 300% in the flow test. The teabag test absorption values at 20 min were selected as this time corresponded to the time when the flow values were measured and was the amount of time the hydrogels had been in the mixture. Generally, a difference in the absorption measurements using the teabag test and the flow test is expected. This difference stems from the fact that in the teabag test hydrogels have access to an infinite amount of solution which is not the case in the flow test and that in the flow test the hydrogels can experience constraints by the surrounding cement mixture. However, the difference in the absorption of Hyd-a and Hyd-b as measured using these two test methods is striking and deserves further investigations. This behavior seemed rather counterintuitive as it would be expected that the difference in the absorption of Hyd-a and Hyd-b be more pronounced in the teabag test compared to the flow test as an infinite solution is available in the case of the teabag test and allows for unhindered absorption of the hydrogels. Nevertheless, a quite opposite behavior was observed. Since Hyd-c did not show such a counterintuitive behavior, in the remainder of our discussion related to absorption, the focus will be on Hyd-a and Hyd-b, and Hyd-c is not considered.

In order to explain the above-mentioned behavior, we hypothesize that the physical and chemical interactions between the solid cement particles and the hydrogels affect the absorption of hydrogels in the flow test. These interactions are not present in the teabag test where the hydrogels absorption is measured in a solution. We sought to investigate the effect of the type of solid particles in the mixture on hydrogel absorption. In addition, the solid particles surrounding hydrogels can impede the free swelling of the hydrogel by exerting mechanical constraint. Thus, both these potential factors were further examined in this paper.

The absorption behavior of Hyd-a and Hyd-b in the ionic solution using the teabag test is depicted in Fig. 3. It is noted that in the ionic solution Hyd-a shows a higher absorption than Hyd-b due primarily to higher pH (> 13) of this solution and a different ionic composition, compared to the extracted pore solution.

Hydrogel absorption in the FA and GP mixtures obtained from the flow test is given in Table 4. It is interesting to note that while the Hyd-b absorption is 19% less than Hyd-a absorption in the ionic solution obtained from the teabag test, the Hyd-b absorption is significantly higher (about 385%) than the Hyd-a absorption in the FA mixture as obtained from the flow test. On the other hand, the Hyd-a absorption is slightly higher than the Hyd-b absorption in the GP mixtures. This observation clearly demonstrated the important role the solid particles play in the absorption of the hydrogels in the mixtures.

3.2 Modified teabag test

The absorption results obtained from the modified teabag test are shown in Fig. 4. The results seemed to

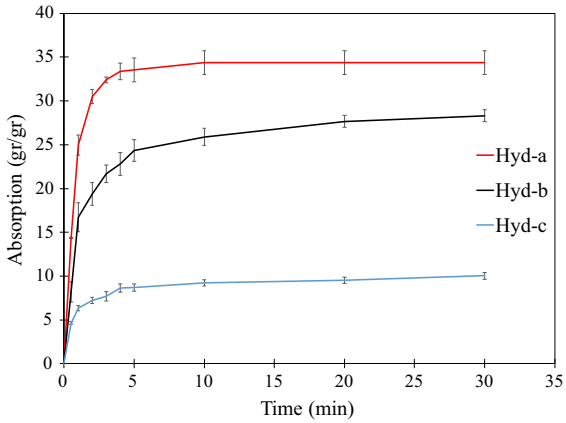

Fig. 3 Absorption of Hyd-a, Hyd-b, and Hyd-c in the ionic solution using the teabag test

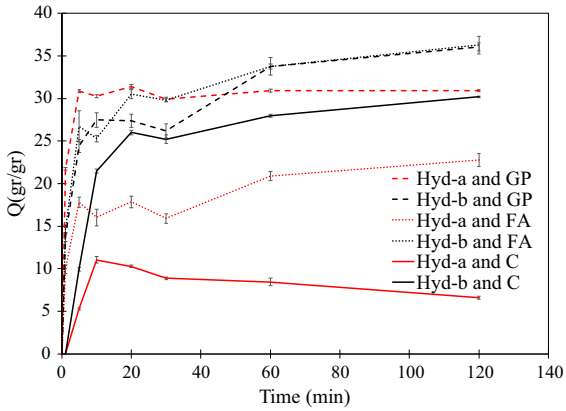

Fig. 4 Absorption results of Hyd-a and Hyd-b obtained from the modified teabag test

be consistent with the absorption results obtained from the flow test (Table 4). It is seen that Hyd-b in the FA mixture showed a higher absorption than Hyd-a. This is in contrast to the higher absorption of Hyd-a compared to Hyd-b in the ionic solution. From Table 4, it is noted that Hyd-a showed a slightly higher absorption than Hyd-b in the GP mixture; this observation appeared to be in agreement with a slightly higher absorption of Hyd-a than Hyd-b from the modified teabag test measured at about 10–20 min, which coincided with the time scale of the flow test. In the case of the cement mixture, Hyd-b demonstrated a noticeably higher absorption than Hyd-a, which was in line with the absorption result obtained from the flow test as shown in Table 3. While a good qualitative agreement was noted between the absorption trends obtained from the flow test and the modified teabag test, there were still quantitative discrepancies between the absorption values from these two tests.

3.3 X-ray micro-CT analysis

Micro-CT analysis was performed to study the macrovoids created as a result of hydrogel absorption in the microstructure of cement pastes during hydration. The size distribution of the macrovoids is plotted in Fig. 5. The average macrovoid size of Hyd-a and Hyd-b was measured to be 384 μm and 775 μm, respectively. 2D visualizations obtained from 3D reconstruction of Hyd-a and Hyd-b are also presented in Fig. 6. It should be reminded that the dry hydrogels used in the mixtures were sieved to have the same initial size range of 75–300 μm. Assuming the average equivalent sphere size of the dry hydrogels to be 187 μm, and using the average equivalent sphere size of the macrovoid in each case, an estimate of the relative volumetric absorption of hydrogels can be made. The volumetric absorption of Hyd-a and Hyd-b are estimated to be 7.6 and 70, respectively. These relative volumetric absorption estimates of the

Table 4 Mix designs of the mixtures used in the modified teabag test

Paste designation	W/C	Superplasticizer (% per cement mass)	Hydrogel (% per cement mass)	Flow (cm)	Absorption (g/g dry)	
					Hyd-a	Hyd-b
FA	0.44	0.5	–	24		
FA Hyd-a	0.48	0.5	0.3	24	13	
FA Hyd-b	0.63	0.5	0.3	24		63
GP	0.38	0.5	–	24		
GP Hyd-a	0.49	0.5	0.3	24	37	
GP Hyd-b	0.47	0.5	0.3	24		30

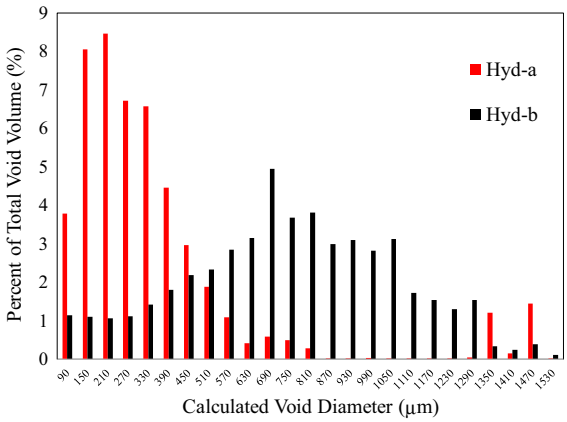

Fig. 5 Macrovoid size distribution of Hyd-a and Hyd-b in cement paste

hydrogels are in a relative agreement with the results obtained from the flow test, in which a significant difference in the absorption of Hyd-a and Hyd-b in the mixture was noted.

The observed behavior of Hyd-a and Hyd-b in the C, FA, and GP mixtures can be attributed to the interactions between hydrogels and the solid particles. It can be postulated that when Hyd-a comes into contact with C or FA particles, chemical interactions occur at the contact surface resulting in a relatively semi-rigid skin on the hydrogel surface reducing the diffusion of the solution into the interior of Hyd-a. On the other hand, Hyd-b seemed to experience the surface chemical reaction to a lesser extent and the diffusion of solution into Hyd-b is not affected to the extent that observed in Hyd-a. On the contrary to C and FA, GP does not seem to react with hydrogels on the contact surface and as a result, the hydrogel absorption behavior is not expected to be affected by the hydrogel/particle chemical interactions and is predominantly governed by the ionic solution. This is evident from Figs. 4 where a higher absorption of Hyd-a than Hyd-b in the first 30 min was observed in the GP mixture and this absorption behavior is also seen in Fig. 3.

3.4 FTIR

FTIR analysis was conducted on the hydrogels to examine the chemical characteristics of the surface of the hydrogels. Figure 7 shows the FTIR spectra of Hyd-a and Hyd-b after absorption in the extracted pore solution and in a cement mixture. The general peaks related to the amide groups (1638 cm^{-1}) [59], asymmetric stretching of the carboxylate (1560 cm^{-1}), and symmetric stretching of the carboxylate groups (1408 cm^{-1}) [30, 60] can be seen in the spectra of the hydrogels. It is seen that the spectra of Hyd-a and Hyd-b in the extracted pore solution showed relatively similar features; however, their spectra in the cement mixture depicted attributes that were different from each other. In addition, these spectra had different attributes than those corresponding to the hydrogels in the extracted pore solution. In the spectra of the hydrogels in the cement mixture, the peak at 874 cm^{-1} is related to out-of-plane bending of CO_3^{-2} [61] and the peak at 1110 cm^{-1} corresponds to the symmetric stretching of CO_3^{-2} [62, 63]. These peaks are absent in the spectra of the hydrogels in the extracted pore

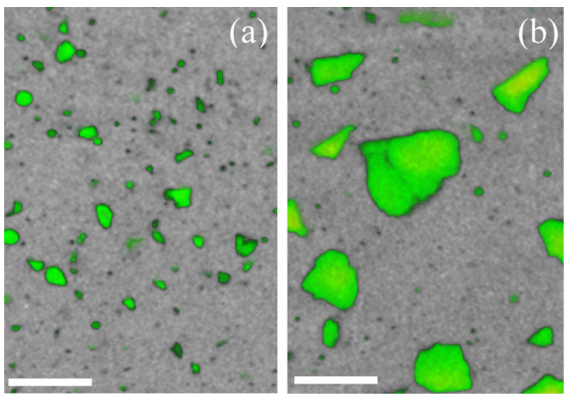

Fig. 6 2D representation obtained from 3D reconstruction of **a** Hyd-a and **b** Hyd-b in cement paste. Macrovoids are shown in green. The scale bar corresponds to 2 mm

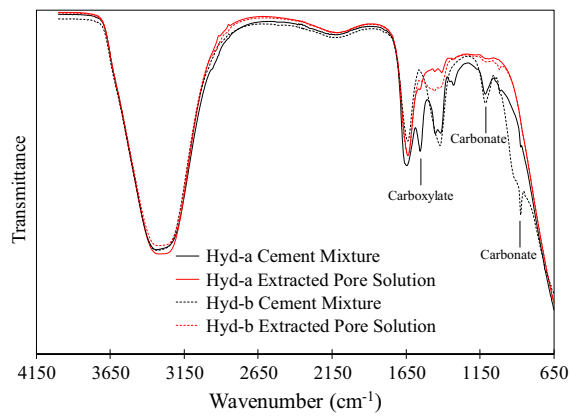

Fig. 7 FTIR spectra of the surface of the Hyd-a and Hyd-b disks in the extracted pore solution and cement mixture

solution. The main difference between the spectra of Hyd-a and Hyd-b in cement mixtures appeared to be the presence of a sharp peak at around 1560 cm^{-1} in the spectrum of Hyd-a and its absence in the spectrum of Hyd-b. The carboxylate groups show a peak at this frequency [60]; however, this peak was weak in Hyd-a in extracted pore solution. It can be hypothesized that the formation of insoluble complexes between negatively charged carboxylate groups and positively charged phases on the surface of the hydrating cement particles increased the concentration of carboxylate groups on the surface of Hyd-a leading to a stronger peak in the FTIR spectrum. It should be emphasized that a more detailed study using other surface characterization techniques, including Scanning Electron Microscopy-Energy Dispersive Spectroscopy (SEM–EDS) and Atomic Force Microscopy (AFM), can be used in order to confirm the above-mentioned hypothesis. The FTIR observations discussed above provide evidence that different chemical interactions occur between Hyd-a and the cement particle than between Hyd-b and the cement particles. Additionally, our previous study using an AFM based nanoindentation technique indicated a slightly higher surface stiffness of Hyd-a than Hyd-b after exposure to cement mixture [55]. Thus, these observations lend more credibility to the argument that the difference in the absorption of Hyd-a and Hyd-b in the extracted pore solution and in cement mixture can be rooted in the difference in the surface characteristics of the hydrogels caused by the chemical interactions between the hydrogels and cement particles.

3.5 Absorption under constraint

In addition to chemical interactions, physical constraint could potentially affect the absorption behavior of hydrogels. In order to examine how physical constraint can affect the absorption behavior of Hyd-a and Hyd-b and if it contributed to the large difference observed in the absorption of Hyd-a and Hyd-b in the mixtures, the absorption measurements were taken under constraint as seen in Fig. 1. The absorption was calculated based on volumetric change and is presented in Fig. 8.

The mechanical constraint exerted on hydrogels from the surrounding mixture affects the absorption of hydrogels and this has been evidenced in our previous study [32, 64] and others [65, 66]. It is seen that the absorption of both Hyd-a and Hyd-b decreased with an increase in the pressure level. The reduction in the absorption of hydrogels due to pressure can be explained from the thermodynamics principle of hydrogel swelling where mechanical pressure is a key factor in determining the hydrogel deformation [66, 67]. An important observation here is that Hyd-a demonstrated a higher absorption than Hyd-b under different pressure levels in the ionic solution. This observation provides evidence that the physical constraints from the mixture is not likely to be a factor in the significantly higher absorption of Hyd-b than Hyd-a in the mixtures. Thus, it can be concluded that the direct chemical interactions between the solid particles and hydrogel is an important mechanism explaining the distinct behavior of hydrogels in the extracted pore solution and in the mixtures. This finding is of significant importance in the internal curing of cementitious materials as the teabag test is commonly used to determine the absorption of hydrogels. As suggested by [51], it should be noted that the chemical composition of the pore solution in a cement mixture varies with time in contrast to the extracted pores solution, which is expected to have a constant chemical composition. Thus, this difference in the chemical composition, could potentially contribute to the large difference observed between the absorption of Hyd-a and Hyd-b in extracted pore solution vs in cement mixture.

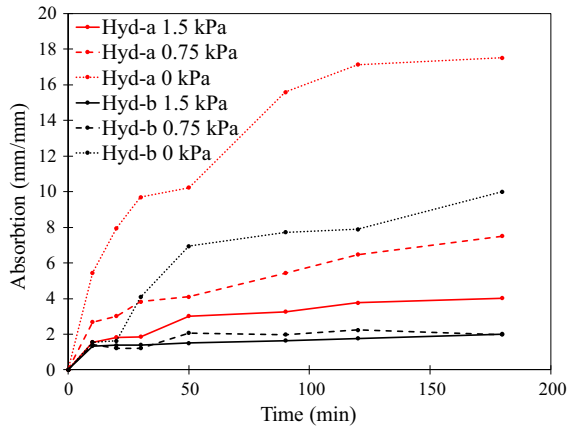

Fig. 8 Absorption of Hyd-a and Hyd-b under three different pressure levels in the ionic solution

3.6 Desorption of hydrogels in cementitious matrix

In this section, the desorption behavior of embedded hydrogel microstrips is presented and discussed. The water loss of the hydrogel microstrips is illustrated in Fig. 9, and the images showing the cross section of Hyd-a, Hyd-b and Hyd-c microstrips at 36 h are shown in Figs. 10a-c, respectively. The image of Hyd-c taken at 168 h is shown in Fig. 10d. In order to account for statistical variability, at least six replicates were used for each hydrogel type and each time. Since the final setting time of the cement mixture in which the hydrogel microstrips were embedded was about 10 h, the desorption measurement of the hydrogel microstrips started at 8 h to cover the time before the final setting and continued until 12, 16, 20, 24 and 36 h. Hyd-c appeared to show a lower desorption rate, and even at 36 h it was still soft, which is evidence that Hyd-c still contained water. Measurements were continued until 48 h only for Hyd-c, which still did not show any loss of water. Hyd-c was examined again after a long time of about one week at which time Hyd-c showed noticeable water loss as depicted in Fig. 10d. All specimens were kept in a sealed condition until examination. In general, the results indicated a higher desorption rate for Hyd-a and Hyd-b compared to Hyd-c. Hyd-a and Hyd-b were almost dried at 24 h but Hyd-c was not dried even at 48 h. The lower desorption rate of Hyd-c compared to Hyd-a and Hyd-b is related to its response to the capillary suction exerted from the matrix. It should be noted that Hyd-c has a smaller cross sectional dimensions compared to Hyd-a and Hyd-b due to a lower absorption capacity of Hyd-c. The smaller dimensions are expected to increase the diffusion rate of water out of the hydrogels but, due to its chemical structure, Hyd-c released the water to the matrix more slowly than Hyd-a and Hyd-b.

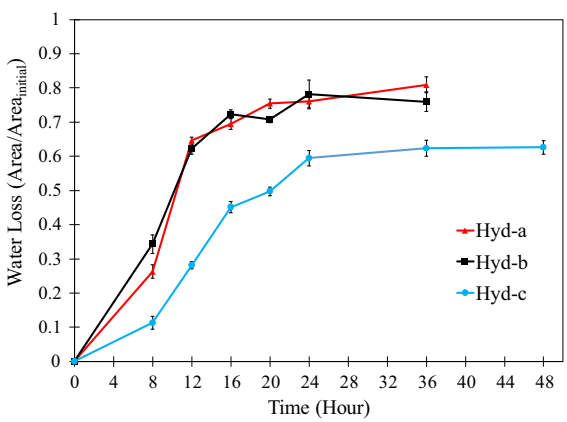

Fig. 9 Water loss of the Hyd-a, Hyd-b, and Hyd-c hydrogel microstrips embedded in cement mixture

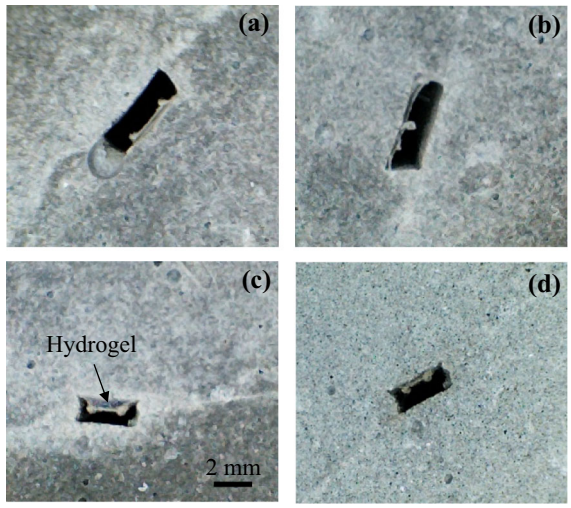

Fig. 10 Micrographs showing the cross section of **a** Hyd-a, **b** Hyd-b, and **c** Hyd-c microstrips, respectively, in cement paste corresponding to 36 h of curing. **d** Micrograph showing the cross section of the Hyd-c microstrip corresponding to 96 h of curing

Hyd-a showed a slightly larger desorption compared to Hyd-b at very early age (8 h); however, Hyd-b demonstrated a faster desorption compared to Hyd-a at 8–12 h. Before 8 h, when the surrounding cementitious matrix had not yet set, the desorption of the hydrogels is primarily due to the chemical interaction between the hydrogel and the pore solution. This explains the larger desorption of Hyd-a than Hyd-b during this time as Hyd-a appeared to be more affected by the chemical interactions. In 8–12 h, which included the final setting time of the cementitious matrix, the capillary forces began to develop and drove the desorption of the hydrogels. The higher desorption of Hyd-b than Hyd-a in 8–12 h can be attributed to more effective influence of the capillary forces on the desorption of Hyd-b than Hyd-a. The effect of the capillary forces on the desorption of hydrogels was studied in detail in our previous papers [55, 68].

3.7 Autogenous shrinkage

Figure 11 shows the results of the autogenous shrinkage of C, C Hyd-a, C Hyd-b, and C Hyd-c. It is seen that the cement pastes with hydrogels were able to reduce shrinkage compared to the control paste, but they showed distinctly different autogenous shrinkage behaviors. In the control paste, a small expansion can be observed after the final setting time, which is the time at which the measurement started. This expansion can be attributed to the crystallization pressure of calcium hydroxide [69]. After this early expansion, C began to shrink until 14 days and after that the shrinkage continued very slowly. During the hydration, water is consumed in cement mixtures, resulting in an increase in self-desiccation and a reduction in relative humidity (RH) in the solid skeleton. Consequently, the reduction in RH increases the capillary pore fluid tensile forces, leading to shrinkage in cementitious matrix [1, 40, 55, 68, 70]. C Hyd-a and C Hyd-b showed a sharp expansion after the setting time; however, the expansion continued until 24 h for C Hyd-b and until 48 h for C Hyd-a. Although not fully understood, the initial expansion in C Hyd-a and C Hyd-b could also be attributed to the crystallization pressure of calcium hydroxide; such expansions in mixes containing hydrogels were also observed by other researchers [36, 62, 91]. The shrinkage of C Hyd-b remained relatively unchanged after the initial expansion; however, C Hyd-a demonstrated a shrinkage after the initial expansion and the rate of the shrinkage is relatively similar to that of C. C Hyd-c showed a completely different trend compared to C Hyd-a and C Hyd-b. It is noted that C Hyd-c showed a very little shrinkage throughout the course of measurement as seen in Fig. 11. The difference in the shrinkage response of the samples containing hydrogels could be related to the absorption and desorption behaviors of the hydrogels. Although a mechanistic explanation of the observed shrinkage behavior cannot be provided at this time and studies are ongoing to investigate this behavior, a comparison with the absorption/desorption results could shed some light on the underlying mechanisms responsible for the shrinkage behavior of the pastes. It is interesting to note the different shrinkage behavior of C Hyd-a and C Hyd-c in spite of the same w/c used in these samples. The small and relatively uniform shrinkage of C Hyd-c could be attributed to the slower desorption of Hyd-c compared to Hyd-a, as seen in Fig. 9. It appears that the slow release of water from Hyd-c allowed for offsetting the reduction in relative humidity in the material as hydration continued and water was consumed. In the case of C Hyd-a, water was released from the hydrogel faster and it can be stipulated that the shrinkage began after the desorption was almost completed. It should be noted that the theoretical amount of entrained water to mitigate self-desiccation for a paste with the base $w/c = 0.35$ is about (w/c) add = 0.06 [6]. Since the amount of additional water in C Hyd-a (0.03) is less than 0.06, it is expected that autogenous shrinkage was not completely mitigated as seen in Fig. 11. On the other hand, the amount of additional water in C Hyd-b (0.13) is noticeably higher than 0.06, and as a result no shrinkage was observed after the initial expansion.

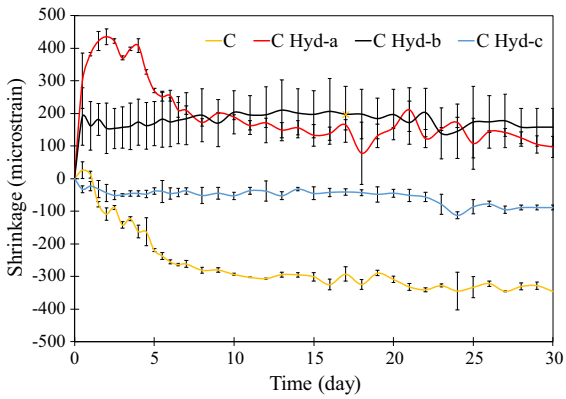

Fig. 11 Autogenous shrinkage of C, C Hyd-a, C Hyd-b, and C Hyd-c

3.8 TGA

TGA/DTG curves of C, C Hyd-a, C Hyd-b, and C Hyd-c are shown in Fig. 12a and b. Major peaks in the DTG curves corresponding to mass losses are identified in Fig. 12b. The mass loss between the room temperature and about 220 °C is attributed to the evaporation of free water and dehydration of the hydrates such as C-S–H and ettringite [71–75]. The second major mass loss took place between 370 °C and 450 °C, and is associated with the dehydroxylation of free calcium hydroxide produced during curing [71–75]. A small mass loss related to decarbonation of calcium carbonate in cement paste occurred between 550 and 750 °C [71–75].

The results of the free calcium hydroxide (CH) content at the age of 3 and 28 days are shown in Fig. 13. An increase in CH content in all cement pastes containing hydrogels is observed at the age of 28 days compared to the Control paste. This increase is attributed to the increased hydration as more water was provided from the hydrogels into the cement paste. The increase in CH content is more pronounced in C Hyd-b than C Hyd-a and C Hyd-c at 28 days, which was expected as the total w/c of C Hyd-b was higher. It is noted that the CH content at 3 days in C Hyd-c is smaller than that in C Hyd-a in spite of the same total w/c. This could be attributed to a slower desorption of Hyd-c than Hyd-a in early age and subsequently slower provision of water to aid in hydration. This observation seemed to be in general agreement with the electrical resistivity results of C Hyd-a and C Hyd-c at early age as discussed in Sect. 3.8.

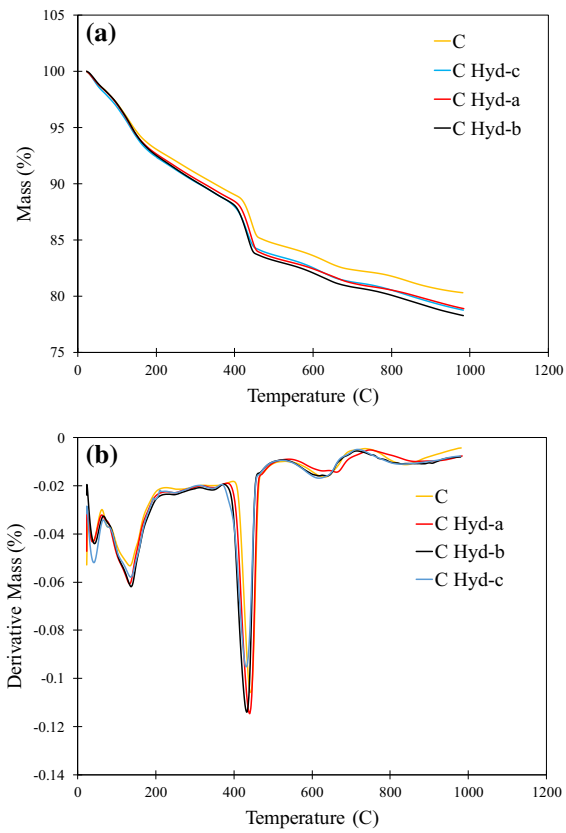

Fig. 12 **a** TGA and **b** DTG curves of C, C Hyd-a, C Hyd-b, and C Hyd-c

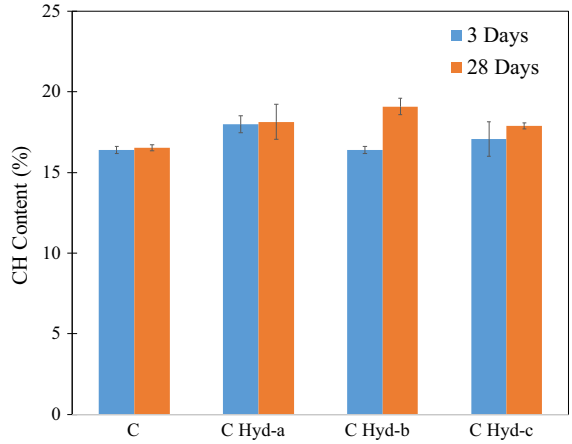

Fig. 13 CH content of C, C Hyd-a, C Hyd-b, and C Hyd-c

3.9 Electrical resistivity

The results of the electrical resistivity measurements of C, C Hyd-a, C Hyd-b, and C Hyd-c at ages of 3, 7, and 28 days are shown in Fig. 14. Electrical resistivity of cementitious materials is dependent on pore structure as well as pore solution resistivity [32, 40, 58, 76–79]. It increases with improved densification of the microstructure and decreases with increasing w/c [32, 40, 58, 76–79]. The electrical resistivity is seen to increase with age as the hydration continued and the microstructure became more densified. It is observed that the pastes with hydrogels showed generally a lower electrical resistivity compared to the control sample. This can be explained in view of higher total w/c of the pastes containing hydrogels. This reduction in electrical resistivity is more pronounced in C Hyd-b which had the highest total w/c. There is a small difference between the electrical resistivity of C Hyd-a and C Hyd-c at 3 and 7 days in spite of the same total w/c in these pastes. The small difference could be attributed to the difference in the desorption rate of Hyd-c and Hyd-a, as previously discussed in Sect. 3.5, and also the difference in the concentration of the hydrogel and size of the macrovoids in the cement paste. The saturation degree of the macrovoids influences electrical resistivity of the pastes. If the macrovoids are fully or partially saturated by hydrogels, they act as an electrical conductor and the electrical conductivity increases. The higher concentration of Hyd-c and its slower desorption compared to Hyd-a could result in a

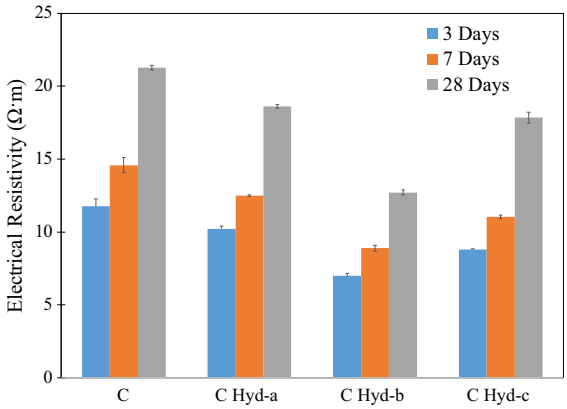

Fig. 14 Electrical resistivity of C, C Hyd-a, C Hyd-b, and C Hyd-c at different ages of curing

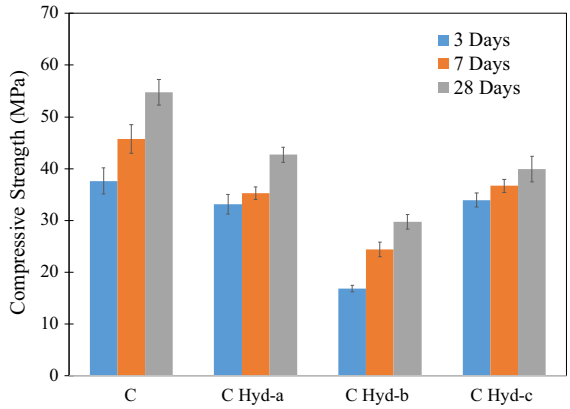

Fig. 15 Compressive strength of C, C Hyd-a, C Hyd-b, and C Hyd-c at different ages of curing

more uniform dispersion of Hyd-c in cement paste and a higher relative humidity in the early age leading to a higher electrical conductivity of C Hyd-c than C Hyd-a at 3 and 7 days. This observation seemed to be in general agreement with the shrinkage results where C Hyd-c demonstrated a lower shrinkage than C Hyd-a as a result of slower desorption of Hyd-c maintaining higher relative humidity compared to Hyd-a. Another contributing factor could be related to the less densified pore structure of C Hyd-c compared to C Hyd-a as a result of slower release of water from Hyd-c into the surrounding cementitious matrix and lower hydration reaction.

3.9.1 Compressive strength

Figure 15 shows the results of compressive strength test of C, C Hyd-a, C Hyd-b, and C Hyd-c at ages of 3, 7, and 28 days. With time and continued curing, the compressive strength of all pastes demonstrated an increase. The addition of hydrogels is seen to decrease compressive strength due primarily to the formation of macrovoids in microstructure, which act as stress concentration sites compromising strength. The largest reduction in compressive strength is seen in C Hyd-b, which contained markedly larger macrovoids compared to C Hyd-a and C Hyd-c, as discussed previously. While the total w/c of C Hyd-a and C Hyd-c was the same, small nuances in the compressive strength of these two pastes can be noted. The main factors responsible for these nuances are the difference in the size and number of macrovoids in these two pastes. The macrovoids in C Hyd-c were smaller in size but larger in number than those in C Hyd-a.

4 Conclusions

The interactions between hydrogels with different chemical compositions and cementitious materials were investigated. Hydrogel absorption measurement in the extracted pore solution using the teabag test can be in a stark contrast to the absorption measurement obtained in cement mixture. The chemical interactions between the hydrating cement particles and hydrogel surface was shown to play an important role in the absorption of hydrogels in cement mixture; formation of a relatively stiff skin on the surface of hydrogel as a result of interactions between the hydrating cement particles and hydrogel can reduce the absorption of hydrogels.

Cement pastes with hydrogels showed a decreased autogenous shrinkage compared to the control paste. The effect of hydrogels on autogenous shrinkage was shown to be dependent on the chemical composition of the hydrogels; the hydrogel with a slow desorption rate demonstrated very low shrinkage in the cement paste. The addition of hydrogels was found to result in a general reduction in the compressive strength and electrical resistivity of cement paste; the formation of macrovoids are responsible for such reductions.

Acknowledgements This study was supported by the National Science Foundation under the CAREER Award Number 1846984 and the MRI Award Number 1920127.

Declarations

Conflict of interest The authors declare that they have no conflict of interest.

References

1. Snoeck D, Jensen OM, De Belie N (2015) The influence of superabsorbent polymers on the autogenous shrinkage properties of cement pastes with supplementary cementitious materials. Cem Concr Res 74:59–67. https://doi.org/10.1016/j.cemconres.2015.03.020
2. de Sensale GR, Goncalves AF (2014) Effects of fine LWA and SAP as internal water curing agents. Int J Concr Struct Mater 8:229–238. https://doi.org/10.1007/s40069-014-0076-1
3. Jensen OM, Hansen PF (2002) Water-entrained cement-based materials II. Experimental observations. Cem Concr Res 32:973–978 https://doi.org/10.1016/S0008-8846(02)00737-8
4. Kovler K, Jensen OM (2007) Internal curing of concrete, state-of-the-art report of RILEM technical committee 196-ICC
5. Schröfl C, Mechtcherine V, Gorges M (2012) Relation between the molecular structure and the efficiency of superabsorbent polymers (SAP) as concrete admixture to mitigate autogenous shrinkage. Cem Concr Res 42:865–873. https://doi.org/10.1016/j.cemconres.2012.03.011
6. Lura P, Jensen OM, Weiss WJ (2009) Cracking in cement paste induced by autogenous shrinkage 1089–1099. https://doi.org/10.1617/s11527-008-9445-z
7. Hossain AB, Weiss J (2004) Assessing residual stress development and stress relaxation in restrained concrete ring specimens 26:531–540.https://doi.org/10.1016/S0958-9465(03)00069-6
8. Mechtcherine V, Gorges M, Schroefl C, Assmann A, Brameshuber W, Ribeiro AB, Cusson D, Custodio J, da Silva EF, Ichimiya K, Igarashi S, Klemm A, Kovler K, Lopez AND, Lura P, Nguyen T, Reinhardt HW, Toledo RD, Weiss J, Wyrzykowski M, Ye G, Zhutovsky S(2014) Effect of internal curing by using superabsorbent polymers (SAP) on autogenous shrinkage and other properties of a high-performance fine-grained concrete: results of a RILEM round-robin test. Mater Struct 541–562. https://doi.org/10.1617/s11527-013-0078-5
9. Jensen OM, Hansen PF (2001) Water-entrained cement-based materials I . Principles and theoretical background. Cem Concr Res 31:647–654
10. Lura P, Jensen OM, van Breugel K (2003) Autogenous shrinkage in high-performance cement paste: An evaluation of basic mechanisms. Cem Concr Res 33:223–232. https://doi.org/10.1016/S0008-8846(02)00890-6
11. Wang K, Jansen DC, Shah SP, Karr AF (1997) Permeability study of cracked concrete. Cem Concr Res 27:381–393
12. Beushausen H, Gillmer M, Alexander M (2014) The influence of superabsorbent polymers on strength and durability properties of blended cement mortars. Cem Concr Compos 52:73–80. https://doi.org/10.1016/j.cemconcomp.2014.03.008
13. Hasholt MT, Jensen OM (2015) Chloride migration in concrete with superabsorbent polymers. Cem Concr Compos 55:290–297. https://doi.org/10.1016/j.cemconcomp.2014.09.023
14. Mechtcherine V, Secrieru E, Schröfl C (2015) Effect of superabsorbent polymers (SAPs) on rheological properties of fresh cement-based mortars—Development of yield stress and plastic viscosity over time. Cem Concr Res 67:52–65. https://doi.org/10.1016/j.cemconres.2014.07.003
15. Snoeck D, Schaubroeck D, Dubruel P, De Belie N (2014) Effect of high amounts of superabsorbent polymers and additional water on the workability, microstructure and strength of mortars with a water-to-cement ratio of 0.50. Constr Build Mater 72:148–157. https://doi.org/10.1016/j.conbuildmat.2014.09.012
16. Montanari L, Suraneni P, Weiss WJ (2017) Accounting for water stored in superabsorbent polymers in increasing the degree of hydration and reducing the shrinkage of internally cured cementitious mixtures. Adv Civ Eng Mater 6:20170098. https://doi.org/10.1520/ACEM20170098
17. Krafcik MJ, Erk KA (2016) Characterization of superabsorbent poly (sodium-acrylate acrylamide) hydrogels and influence of chemical structure on internally cured mortar. Mater Struct 49:4765–4778. https://doi.org/10.1617/s11527-016-0823-7
18. Soliman AM, Nehdi ML (2011) Effect of drying conditions on autogenous shrinkage in ultra-high performance concrete at early-age. Mater Struct 44:879–899. https://doi.org/10.1617/s11527-010-9670-0
19. Cusson D, Hoogeveen T (2008) Internal curing of high-performance concrete with pre-soaked fine lightweight aggregate for prevention of autogenous shrinkage cracking. Cem Concr Res 38:757–765. https://doi.org/10.1016/j.cemconres.2008.02.001
20. Şahmaran M, Lachemi M, Hossain KMA, Li VC (2009) Internal curing of engineered cementitious composites for prevention of early age autogenous shrinkage cracking. Cem Concr Res 39:893–901. https://doi.org/10.1016/j.cemconres.2009.07.006
21. Bentur A, Igarashi S, Kovler K (2001) Prevention of autogenous shrinkage in high-strength concrete by internal curing using wet lightweight aggregates. Cem Concr Res 31:1587–1591. https://doi.org/10.1016/S0008-8846(01)00608-1
22. Mechtcherine V, Reinhardt H-W (2012) Application of Super Absorbent Polymers (SAP) in concrete construction, Springer
23. Jensen OM, Lura P (2006) Techniques and materials for internal water curing of concrete. Mater Struct Constr 39:817–825. https://doi.org/10.1617/s11527-006-9136-6
24. Hasholt MT, Jensen OM, Kovler K, Zhutovsky S (2012) Can superabsorent polymers mitigate autogenous shrinkage of internally cured concrete without compromising the strength? Constr Build Mater 31:226–230. https://doi.org/10.1016/j.conbuildmat.2011.12.062
25. Lura P, Durand F, Loukili A, Kovler K (2006) Compressive strength of cement pastes and mortars with superabsorbent polymers. In: Int. RILEM Conf. Vol. Chang. Hardening

Concr. Test. Mitig. 20–23 August, 2006: pp 117–125. https://doi.org/10.1617/2351580052.013
26. Igarashi S, Watanabe A, Jensen OM, Lura P, Kovler K (2006) Experimental study on prevention of autogenous deformation by internal curing using super-absorbent polymer particles. In: Jensen OM, Lura P, Kovler K (eds) RILEM Publications, Gabneus (France), 2006: pp 77–86. https://doi.org/10.1617/2351580052.009
27. Mönnig S, Lura P (2007) Superabsorbent polymers—an additive to increase the freeze-thaw resistance of high strength concrete. Adv Constr Mater 351–358. https://doi.org/10.1007/978-3-540-72448-3_35
28. Snoeck D, Steuperaert S, Van Tittelboom K, Dubruel P, De Belie N (2012) Visualization of water penetration in cementitious materials with superabsorbent polymers by means of neutron radiography. Cem Concr Res 42:1113–1121. https://doi.org/10.1016/j.cemconres.2012.05.005
29. Lee HXD, Wong HS, Buenfeld NR (2016) Self-sealing of cracks in concrete using superabsorbent polymers. Cem Concr Res 79:194–208. https://doi.org/10.1016/j.cemconres.2015.09.008
30. Mignon A, Graulus GJ, Snoeck D, Martins J, De Belie N, Dubruel P, Van Vlierberghe S (2014) pH-sensitive superabsorbent polymers: a potential candidate material for self-healing concrete. J Mater Sci 50:970–979. https://doi.org/10.1007/s10853-014-8657-6
31. Pourjavadi A, Fakoorpoor SM, Hosseini P, Khaloo A (2013) Interactions between superabsorbent polymers and cement-based composites incorporating colloidal silica nanoparticles. Cem Concr Compos 37:196–204. https://doi.org/10.1016/j.cemconcomp.2012.10.005
32. Farzanian K, Pimenta Teixeira K, Perdiago Rocha I, De Sa Carneiro L, Ghahremaninezhad A (2016) The mechanical strength, degree of hydration, and electrical resistivity of cement pastes modified with superabsorbent polymers. Constr Build Mater 109:156–165. https://doi.org/10.1016/j.conbuildmat.2015.12.082
33. Wehbe Y, Ghahremaninezhad A (2017) Combined effect of shrinkage reducing admixtures (SRA) and superabsorbent polymers (SAP) on the autogenous shrinkage and properties of cementitious materials. Constr Build Mater 138:151–162. https://doi.org/10.1016/j.conbuildmat.2016.12.206
34. Hasholt MT, Jesperson MHS, Jensen OM (2010) Mechanical properties of concrete with SAP part I: Development of compressive strength. In: Jensen OM, Hasholt MT, Laustsen S (eds) Int. RILEM Publications SARL, RILEM Conf. Use Superabsorbent Polym. Other New Addit. Concr., pp 117–126
35. Esteves LP (2011) Superabsorbent polymers: On their interaction with water and pore fluid. Cem Concr Compos 33:717–724. https://doi.org/10.1016/j.cemconcomp.2011.04.006
36. Zhu Q, Barney CW, Erk KA (2015) Effect of ionic crosslinking on the swelling and mechanical response of model superabsorbent polymer hydrogels for internally cured concrete. Mater Struct 48:2261–2276. https://doi.org/10.1617/s11527-014-0308-5
37. Horkay F, Tasaki I, Basser PJ (2000) Osmotic swelling of polyacrylate hydrogels in physiological salt solutions. Biomacromol 1:84–90. https://doi.org/10.1021/bm9905031
38. Siriwatwechakul W, Siramanont J, Vichit-Vadakan W (2012) Behavior of superabsorbent polymers in calcium- and sodium-rich solutions. J Mater Civ Eng 24:976–980. https://doi.org/10.1061/(ASCE)MT.1943-5533.0000449
39. Farzanian K, Ghahremaninezhad A (2018) On the effect of chemical composition on the desorption of superabsorbent hydrogels in contact with a porous cementitious material. Gels 4:70. https://doi.org/10.1617/s11527-017-1068-9
40. Vafaei B, Farzanian K, Ghahremaninezhad A (2020) The influence of superabsorbent polymer on the properties of alkali-activated slag pastes. Constr Build Mater 236:117525. https://doi.org/10.1016/j.conbuildmat.2019.117525
41. Krafcik MJ, Macke ND, Erk KA (2017) Improved concrete materials with hydrogel-based internal curing agents. Gels 3:46. https://doi.org/10.3390/gels3040046
42. Krafcik MJ, Bose B, Erk KA (2018) Synthesis and characterization of polymer-silica composite hydrogel particles and influence of hydrogel composition on cement paste microstructure. Adv Civ Eng Mater 7:590–613. https://doi.org/10.1520/ACEM20170144
43. Schroefl C, Mechtcherine V, Vontobel P, Hovind J, Lehmann E (2015) Sorption kinetics of superabsorbent polymers (SAPs) in fresh Portland cement-based pastes visualized and quantified by neutron radiography and correlated to the progress of cement hydration. Cem Concr Res 75:1–13. https://doi.org/10.1016/j.cemconres.2015.05.001
44. Snoeck D, Velasco LF, Mignon A, Van Vlierberghe S, Dubruel P, Lodewyckx P, De Belie N (2015) The effects of superabsorbent polymers on the microstructure of cementitious materials studied by means of sorption experiments. Cem Concr Res 77:26–35
45. Snoeck D, Schaubroeck D, Dubruel P, De Belie N (2014) Effect of high amounts of superabsorbent polymers and additional water on the workability, microstructure and strength of mortars with a water-to-cement ratio of 0.50. Constr Build Mater 72:148–157
46. Schröfl C, Snoeck D, Mechtcherine V (2017) A review of characterisation methods for superabsorbent polymer (SAP) samples to be used in cement-based construction materials: report of the RILEM TC 260-RSC. Mater Struct 50:197. https://doi.org/10.1617/s11527-017-1060-4
47. Mechtcherine V, Snoeck D, Schröfl C, De Belie N, Klemm AJ, Ichimiya K, Moon J, Wyrzykowski M, Lura P, Toropovs N, Assmann A, Ichi Igarashi S, De La Varga I, Almeida FCR, Erk K, Ribeiro AB, Custódio J, Reinhardt HW, Falikman V (2018) Testing superabsorbent polymer (SAP) sorption properties prior to implementation in concrete: results of a RILEM Round-Robin Test. Mater Struct Constr 51. https://doi.org/10.1617/s11527-018-1149-4
48. Kamali M, Ghahremaninezhad A (2017) An investigation into the influence of superabsorbent polymers on the properties of glass powder modified cement pastes. Constr Build Mater 149:236–247
49. Esteves LP (2015) Recommended method for measurement of absorbency of superabsorbent polymers in cement-based materials. Mater Struct Constr 48:2397–2401. https://doi.org/10.1617/s11527-014-0324-5

50. Assmann A (2013) Physical properties of concrete modified with superabsorbent polymers, University of Stuttgart
51. Zhao S, Jensen OM, Hasholt MT (2020) Measuring absorption of superabsorbent polymers in cementitious environments. Mater Struct Constr 53:1–16. https://doi.org/10.1617/s11527-020-1442-x
52. Zhao S, Jensen OM, Hasholt MT, Guan X (2021) Absorption capacity of superabsorbent polymer in cement pastes: a robustness test. Mater Struct Constr 54:1–15. https://doi.org/10.1617/s11527-021-01636-7
53. Justs J, Wyrzykowski M, Bajare D, Lura P (2015) Internal curing by superabsorbent polymers in ultra-high performance concrete. Cem Concr Res 76:82–90. https://doi.org/10.1016/j.cemconres.2015.05.005
54. Lin DC, Dimitriadis EK, Horkay F (2007) Robust strategies for automated AFM force curve analysis-II: adhesion-influenced indentation of soft, elastic materials. J Biomech Eng 129:904–912. https://doi.org/10.1115/1.2800826
55. Farzanian K, Ghahremaninezhad A (2018) Desorption of superabsorbent hydrogels with varied chemical compositions in cementitious materials. Mater Struct Constr 51. https://doi.org/10.1617/s11527-017-1128-1
56. Tunstall LE, Scherer GW, Prud'homme RK (2017) Studying AEA interaction in cement systems using tensiometry. Cem Concr Res 92:29–36. https://doi.org/10.1016/j.cemconres.2016.11.005
57. Jain JA, Neithalath N (2010) Chloride transport in fly ash and glass powder modified concretes—influence of test methods on microstructure. Cem Concr Compos 32:148–156. https://doi.org/10.1016/j.cemconcomp.2009.11.010
58. Neithalath N, Weiss J, Olek J (2006) Characterizing Enhanced Porosity concrete using electrical impedance to predict acoustic and hydraulic performance. Cem Concr Res 36:2074–2085. https://doi.org/10.1016/j.cemconres.2006.09.001
59. Chavda HV, Patel RD, Modhia IP, Patel CN (2012) Preparation and characterization of superporous hydrogel based on different polymers. Int J Pharm Investig 2:134
60. Mignon A, Snoeck D, Schaubroeck D, Luickx N, Dubruel P, Van Vlierberghe S, De Belie N (2015) pH-responsive superabsorbent polymers: a pathway to self-healing of mortar. React Funct Polym 93:68–76. https://doi.org/10.1016/j.reactfunctpolym.2015.06.003
61. Xia M-S, Yao Z-T, Ge L-Q, Chen T, Li H-Y (2014) A potential bio-filler: The substitution effect of furfural modified clam shell for carbonate calcium in polypropylene. J Compos Mater 49:807–816. https://doi.org/10.1177/0021998314525981
62. Fernández-Carrasco L, Torrens-Martín D, Morales LM, Sagrario Martínez-Ramírez (2012) Infrared spectroscopy in the analysis of building and construction materials. Infrared Spectrosc—Mater Sci Eng Technol Technol 370:369–382. https://doi.org/10.5772/36186
63. Chu DH, Vinoba M, Bhagiyalakshmi M, Baek IH, Nam SC, Yoon Y, Kim SH, Jeong SK (2013) CO2 mineralization into different polymorphs of CaCO3 using an aqueous-CO2 system. RSC Adv 3:21722–21729. https://doi.org/10.1039/C3RA44007A
64. Farzanian K, Wehbe Y, Ghahremaninezhad A (2016) The effect of superabsorbent polymers (sap) on the performance of cementitious materials. In: 4th Int. Conf. Sustain. Constr. Mater. Technol
65. Louf J, Lu NB, Connell MGO, Cho HJ, Datta SS (2021) Under pressure: Hydrogel swelling in a granular medium 1–11
66. Yoon J, Cai S, Suo Z, Hayward RC (2010) Poroelastic swelling kinetics of thin hydrogel layers: comparison of theory and experiment. Soft Matter 6:6004. https://doi.org/10.1039/c0sm00434k
67. Marcombe R, Cai S, Hong W, Zhao X, Lapusta Y, Suo Z (2010) A theory of constrained swelling of a pH-sensitive hydrogel. Soft Matter 6:784. https://doi.org/10.1039/b917211d
68. Farzanian K, Ghahremaninezhad A (2017) The effect of the capillary forces on the desorption of hydrogels in contact with porous cementitious material. Mater Struct 50:216. https://doi.org/10.1617/s11527-017-1068-9
69. Sant G, Lothenbach B, Juilland P, Le Saout G, Weiss J, Scrivener K (2011) The origin of early age expansions induced in cementitious materials containing shrinkage reducing admixtures. Cem Concr Res 41:218–229. https://doi.org/10.1016/j.cemconres.2010.12.004
70. Farzanian K, Vafaei B, Ghahremaninezhad A (2019) The behavior of superabsorbent polymers (SAPs) in cement mixtures with glass powders as supplementary cementitious materials. Materials (Basel) 12. https://doi.org/10.3390/ma12213597
71. Tobón JI, Payá JJ, Borrachero MV, Restrepo OJ (2012) Mineralogical evolution of Portland cement blended with silica nanoparticles and its effect on mechanical strength. Constr Build Mater 36:736–742
72. Senff L, Labrincha JA, Ferreira VM, Hotza D, Repette WL (2009) Effect of nano-silica on rheology and fresh properties of cement pastes and mortars. Constr Build Mater 23:2487–2491. https://doi.org/10.1016/j.conbuildmat.2009.02.005
73. Esteves LP (2011) On the hydration of water-entrained cement–silica systems: Combined SEM, XRD and thermal analysis in cement pastes. Thermochim Acta 518:27–35
74. Wu L, Zhang Z, Yang M, Yuan J, Li P, Men X (2020) Graphene enhanced and in situ-formed alginate hydrogels for reducing friction and wear of polymers. Colloids Surfaces A Physicochem Eng Asp. https://doi.org/10.1016/j.colsurfa.2020.124434
75. Ashraf M, Khan AN, Ali Q, Mirza J, Goyal A, Anwar AM (2009) Physico-chemical, morphological and thermal analysis for the combined pozzolanic activities of minerals additives. Constr Build Mater 23:2207–2213
76. Jain J, Neithalath N (2011) Electrical impedance analysis based quantification of microstructural changes in concretes due to non-steady state chloride migration. Mater Chem Phys 129:569–579. https://doi.org/10.1016/j.matchemphys.2011.04.057
77. Bu Y, Weiss J (2014) The influence of alkali content on the electrical resistivity and transport properties of cementitious materials. Cem Concr Compos 51:49–58. https://doi.org/10.1016/j.cemconcomp.2014.02.008
78. Rajabipour F, Sant G, Weiss J (2007) Development of electrical conductivity-based sensors for health monitoring of concrete materials. In: TRB Annu. Conf., 2007: p 16.

79. Neithalath N, Weiss J, Olek J (2006) Predicting the permeability of pervious concrete (enhanced porosity concrete) from non-destructive electrical measurements, 2006, Purdue University, rmcfoundation.org